Observations of Breakup Processes of Liquid Jets Using Real-Time X-Ray Radiography

J. M. Char,* K. K. Kuo,† and K. C. Hsieh‡
The Pennsylvania State University, University Park, Pennsylvania

Liquid jet breakup mechanisms and processes have been studied extensively over the last 50 years. However, since the region near the jet injector is too dense and optically opaque, conventional visualization cannot be applied with satisfactory experimental results. To unravel the liquid jet breakup process in the nondilute region, a newly developed system of real-time x-ray radiography together with an advanced digital image processor and a high-speed video camera was used in this study. Based upon recorded x-ray images, the inner structure of a liquid jet during breakup was observed. The jet divergent angle, jet breakup length, and void fraction distributions along the axial and transverse directions of liquid jets were determined in the near-injector region. Both wall- and free-jet tests were conducted to study the effect of wall friction on the jet breakup process.

Nomenclature

H = gap width of the liquid jet at the exit plane
I = x-ray intensity
I_0 = x-ray intensity for the region unintercepted by liquid
L = local interception length
L_{CB} = jet core breakup distance
L_{SB} = jet surface breakup distance
m = linear attenuation coefficient of photoelectric absorption
u = jet head velocity component in x direction
v = jet head velocity component in y direction
W = local sum of the intercepted width of the liquid in the two-phase jet
x = horizontal coordinate along the flow direction
y = vertical coordinate perpendicular to the flow direction
θ = jet spread angle
ϕ = local void fraction

Introduction

UNDERSTANDING the breakup mechanism of liquid jets in diesel engines, regenerative liquid propellant guns, and many other combustion and propulsion systems is extremely important since the jet breakup process can strongly affect the jet divergent angle, the distributions of droplet size and velocity, and the mixing and combustion processes. As indicated in a detailed review paper by Arcoumanis and Whitelaw,[1] numerous theoretical and experimental attempts have been made to study the stability and breakup phenomena of liquid jets ejected from nozzles. In recent years, Wu et al.,[2] Birk and Reeves,[3] and Baev et al.[4] conducted intensive studies in the experimental investigation of breakup behavior in the near-injector region. Shimizu et al.[5] studied the breakup length of a high-speed jet by measuring the electrical resistance between a nozzle and a fine wire detector located in a spray jet. They found that breakup length decreases with increase in injection velocity, finally reaching a constant value.

In the theoretical analyses, the growth of initial perturbations on the liquid surface and the effects of liquid inertia, surface tension, and viscous and aerodynamic forces on the jet were considered. The earliest development of a predictive model for the jet breakup was initiated by Rayleigh.[6,7] His linear stability analysis of an inviscid cylindrical liquid jet showed that an axisymmetric disturbance could be stable or unstable, depending upon whether its wavelength is less or greater than the circumference of the jet. Further investigations using linear stability analysis were conducted by Tyler and Richardson,[8] Schweitzer,[9] Merrington,[10] Levich,[11] Dombrowski and Hooper,[12] and others. Based on these studies, the jet divergent angle near the injector exit and the jet breakup length and mean drop size near the lateral surface of the jet can be estimated from the Reynolds number, the Weber number, the density ratio of liquid to gas, and several empirical constants. The effect of viscosity was studied by Weber.[13] More recently, the effect of nonlinearity[14-19] has been considered and solved numerically in order to simulate more closely the jet breakup processes.

The structure of pressure-atomized sprays was studied by Ruff et al.[20] using water jets in still air at atmospheric pressure. Distributions of mean liquid volume fractions were measured using gamma-ray absorption. They found that mixing depended strongly on the degree of flow development and turbulence levels at the injector exit. Fully developed injector flow and atomization breakup yielded the fastest mixing rates.

In the experimental studies, the core of the jet is optically opaque due to the high-density condition in the near-injector region. Hence, observations and measurements of the near-injector region are almost impossible. Consequently, most previous studies focused on the dilute region or on the jet boundary near the injector exit.[2] Due to the lack of quantitative test results in the near-injector region, the theoretical models developed for prediction of jet-core breakup length, mean drop size distribution, etc., have not yet been validated. The estimated jet profiles and characteristics at a given near-injector station were used as initial and/or boundary conditions in order to simulate the atomization and combustion processes in the dilute region; this, in turn, could cause errors and uncertainties in the theoretical predictions of combustion processes.

The purpose of the present study is to achieve a better understanding of the jet breakup process using a newly developed system of real-time, x-ray radiography together with an advanced digital image processor and a high-speed video camera. The specific objectives are 1) to illustrate the differences between x-ray radiography images and regular high-speed movie films; 2) to measure jet velocity, jet breakup length, and void fraction distributions in the near-injector region; 3) to observe

*Ph.D. Student, Department of Mechanical Engineering; currently, Associate Professor of Chinese Air Force Academy, Taiwan, R.O.C.
†Distinguished Professor of Mechanical Engineering. Associate Fellow AIAA.
‡Research Assistant, Department of Mechanical Engineering; currently, Sverdrup Technology, Inc., Cleveland, Ohio.

the evolution of the jet breakup and the formation of liga-
ments and droplets in the near-injector region in order to
determine the inner structure of the liquid jets; and 4) to
demonstrate the feasibility and advantage of using x-ray radio-
graphy in the jet breakup study. In order to study the effect of
wall friction on the jet breakup process, both wall- and free-jet
tests were conducted.

Experiment Apparatus

In the experimental approach, a test rig has been designed
and fabricated to simulate both wall and free jets ejected from
a two-dimensional slit with an aspect ratio of 10. The advan-
tage of using a planar two-dimensional jet is to avoid the
curvature effect which is inherently associated wth circular or
annular jets.[3] The side view of the jet breakup process is much
clearer in the planar two-dimensional case than in other cases.

The schematic diagram of the test rig is shown in Fig. 1. In Fig.
1, the gap of the two-dimensional slit between elements 5 and
7 is 2 mm, and element 5 is an interchangeable piece for
providing different lengths of the wall jet. When a piece of
element 5 ends at the same location as element 7, the configu-
ration is that of a free-jet test case. A pressure transmitting rod
is shown as element 4. Prior to the test, this rod was lifted by
a vacuum pump. The liquid was then loaded through element
6 into the free volume beneath the rod and the entire slit
region. The liquids used in tests were either water or Pan-
topaque ($C_{19}H_{29}IO_2$), a fluid used in medical x-ray examina-
tions. The physical properties of the two test fluids are pre-
sented in Table 1. During the test, a solenoid valve was
activated to introduce high-pressure nitrogen gas into the top
portion of the test rig that pushes the rod downward to inject
the liquid into the unconfined ambient air. A major portion of
the Pantopaque was recovered for further use.

Data Acquisition System

During the test, the instantaneous liquid jet contour was
filmed by real-time, x-ray radiography. Figure 2 shows the
layout of various components of the radiography system. A
continuous x ray was generated from the Phillips MG 321
constant potential x-ray system. Two x-ray tubes [one with a
focal spot combination of 0.2×0.2 mm/3×3 mm (MCN 167/
160 kV), the other with a focal spot combination of 1.2×1.2
mm/4×4 mm (MCN 321/320 kV)] were employed to achieve
different penetration depths and spatial resolution require-
ments. It is useful to note that the focal spot of the x-ray tube
is the area on the anode which emits x-ray photons. The x-ray
radiography system has options for two different sized focal
spots. The selection is achieved by flipping an electrical switch.
A lead diaphragm was installed at the exit port of the x-ray
tube head to limit the angle of divergence of the x-ray beam
and to confine the beam to the measuring section of the liquid
jet test rig. (This also reduced unnecessary radiation exposure.)
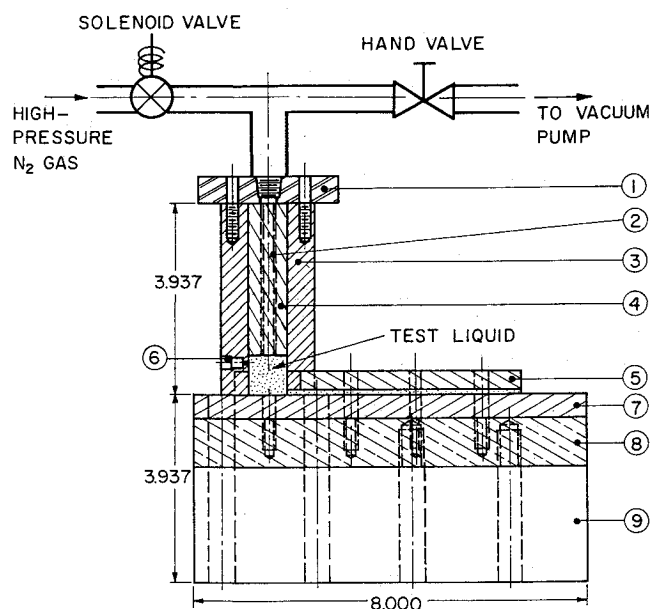A second lead diaphragm with a larger opening was placed in

Fig. 1   Schematic diagram of test rig assembly for two-dimensional
wall or free jet breakup studies 1) top cover, 2) bolts, 3) liquid reser-
voir, 4) push rod, 5) top plate of slit, 6) liquid feeding hole, 7) base
plate of slit, 8) and 9) test rig holder.

Table 1   Physical properties of test liquids

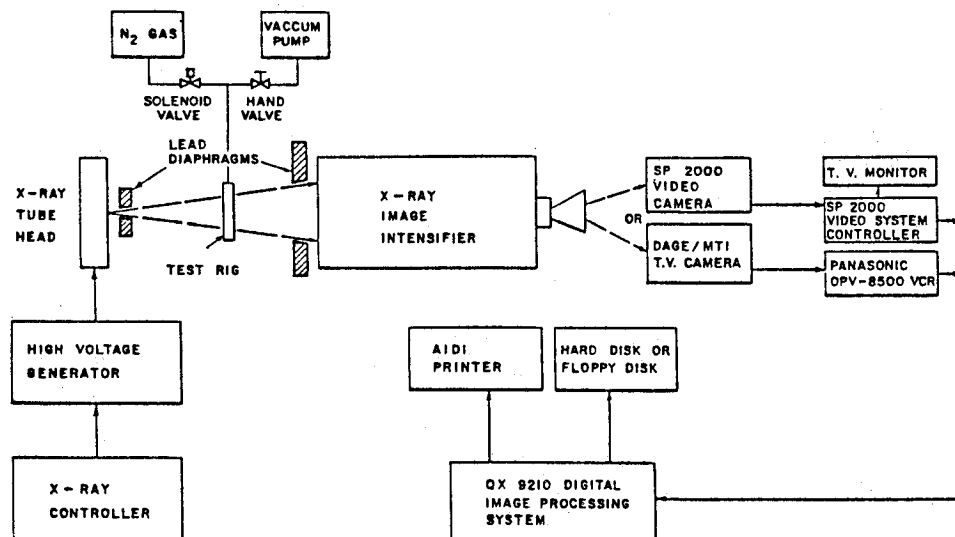| Type	Viscosity, poise	Density, gm/cm^3	Surface tension, dynes/cm
Water	0.01	1.0	72.7
Pantopaque ($C_{19}H_{29}IO_2$)	0.051	1.259	32.1

Fig. 2   Real-time, x-ray radiography and digital image processing system.

front of the image intensifier to reduce scattered x-ray radiation and decrease the noise level on the fluorescent screen.

After passing through the test rig and liquid jet, x-ray signals were transformed to fluorescent light signals on the output screen of a tri-field image intensifier (Precise Optics, Model P1 2400 ATF, 4-in., 6-in., or 9-in. field diameter). The input fluor of the image intensifier was made of cesium iodide with a decay-time constant of 650 ns, and the output fluor was a p20 type with a 85-ns decay-time constant. These time constants are short enough to allow the motion analysis system to operate at its maximum framing rate without generating image blur.

The fluorescent light signal output from the image intensifier was recorded by a Spin Physics 2000 Motion Analysis System. This system can record up to 2000 fully digitized frames/s or up to 12,000 digitized pictures/s with adjustable playback speed. The motion analysis system consists of the following subsystems:

1) a Spin Physics 2000 video camera with solid-state image sensor (the picture information goes to the console from the camera and is processed into a frequency-modulated carrier that is recorded on tape);

2) a main electronic bin, which contains record and playback electronics along with video output circuitry; and

3) a tape transport, which drives the half-inch tape cassette at a maximum speed of 250 in./s.

Digitized data were stored on a high-intensity magnetic recording tape and transferred to the digital image-processing system frame by frame for analysis through an IEEE-488 interface. The digital image-processing system consists of several major components:

1) A Quantex (QX-9210) digital image processor with two pipeline point processors, each with a random access image memory of $480 \times 640 \times 12$ bits. (The processors perform real-time image enhancements, including noise reduction, image subtraction, arbitrary contrast control, roam, and zoom. The processor can also be used to conduct such high-speed image analyses as brightness histogram, local contrast stretch, area and point brightness measurements, calibrated length and area measurements, Sobel edge enhancement, and so forth.)

2) A mass storage device consisting of both a 2.4-MB dual 8-in. floppy diskette drive and a 50-MB hard disk for storage of image data.

3) A high-resolution videograph printer (AIDI CT1500) for producing large high-quality pictures on hard copies with 1660 lines/in. resolution.

Data Reduction Procedure

Besides observing the jet structure directly from the recorded film (both regular movie and x-ray films), more detailed and accurate data could be deduced by analyzing the x-ray intensity distribution across the jet in horizontal and vertical directions. Basically, an ideal radiography image of the liquid jet can be determined from the assumptions that 1) x-ray radiation is generated from a point source via an infinitely small focal spot, 2) x ray is only attenuated by photoelectric absorption, and 3) distribution of x-ray intensity over the input screen of an image intensifier is uniform. As shown in Fig. 3, the x-ray intensity distribution on a y = constant plane can be evaluated by the following equation:

$$I(x) = I_0 \exp\left[-mW(x) \right] \qquad (1)$$

where m is the linear attenuation coefficient of photoelectric absorption, and $W(x)$ is the local sum of the intercepted width of the liquid in the two-phase jet. Due to the x-ray beam attenuation across the liquid jet, the following test data can be obtained using the digital image-processing system.

1) Measurement of radiance intensity or pixel value: The radiance intensity (or pixel value) of any arbitrary point of interest in the jet can be obtained by moving the cursor to that
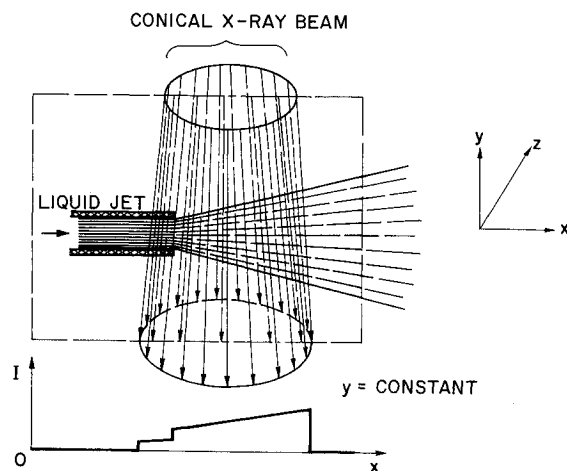

Fig. 3 X-ray intensity distribution across a liquid jet under idealized conditions.
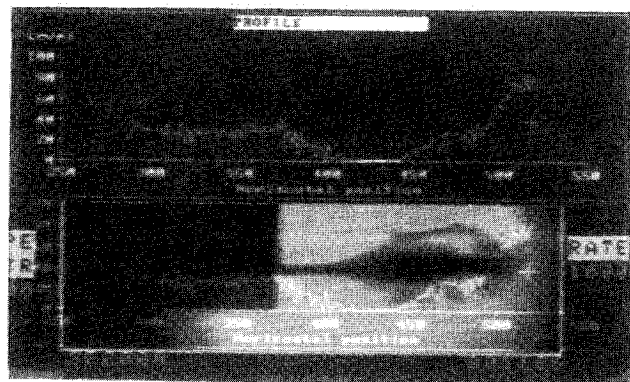

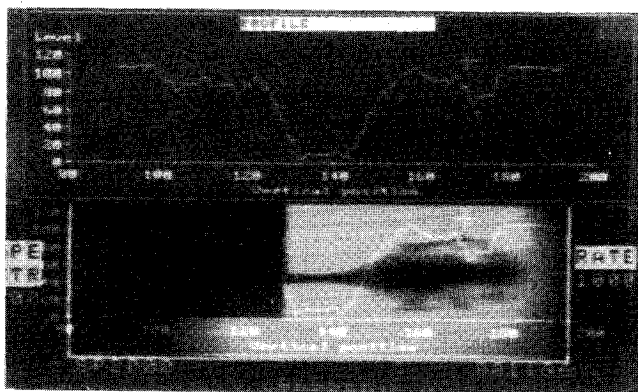Fig. 4 Horizontal x-ray intensity profile at the center plane of a liquid jet.

Fig. 5 Vertical x-ray intensity profile at a distance from jet exit.

point. The local radiance and the x,y coordinates of the location can be displayed on the screen.

2) Measurement of area and pixel value: The software program combines a measurement of an area with a measurement of the integrated pixel values (or total radiance) within the area. The calculated average pixel value within the area is also displayed on the screen. This feature can be used to detect the local void fraction level from the x-ray radiograph for a specified jet region.

3) Profile analysis: Figures 4 and 5 show the measurement of the pixel value of two scan lines—one parallel and one perpendicular to the jet core and head regions. Both end at the
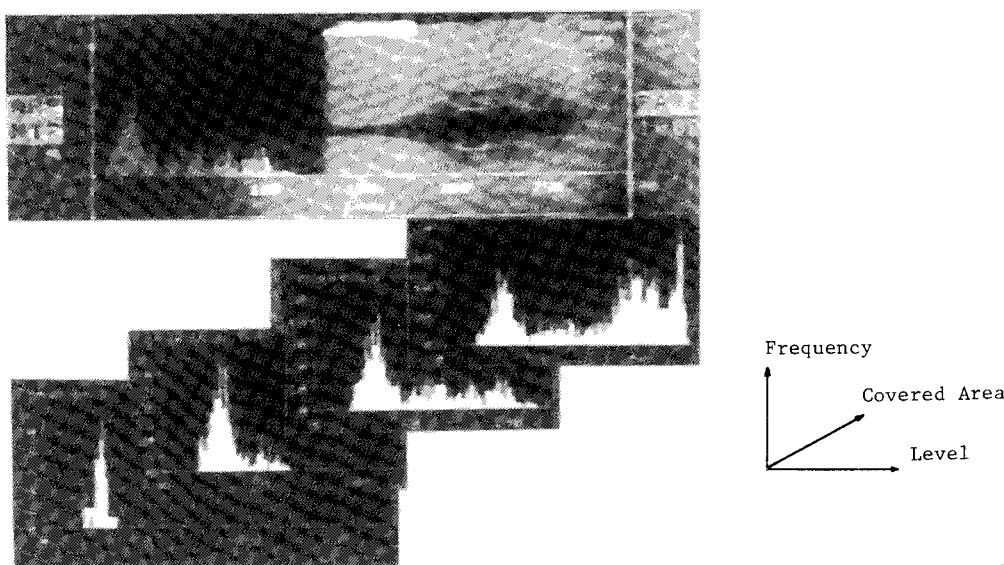
Fig. 6   Histogram analysis on different selected area of a liquid jet.

cursor point. From these profiles, the void-fraction distribution can be deduced for a certain cross section of the jet.

4) Histogram analysis: This procedure consists of measuring the frequency of occurrence of pixel values within a selected boundary of a rectangle. Such distributions can be used to detect jet breakup phenomena in the core region. Keeping the axial length of rectangular area constant by varying the width of the rectangle, different sets of histograms can be obtained. These are arranged into a series of histograms (see Fig. 6).

5) Isophote analysis: Using the data reduction program, certain regions of the viewing area with the same range of pixel values can be replaced by white spots. This feature makes it possible to observe the contours of different radiances. The inner structure of a liquid jet can, therefore, be studied by selecting different pixel values (see Fig. 10, to be discussed later in the results section).

The jet-head velocities in both axial and radial directions can be deduced from the recorded film by using the elapsed time and displacement of reticle lines on the monitor of the Spin Physics Camera System. In terms of spatial and temporal resolutions, the minimum particle size that can be observed by the present system is about 125 μm, and the time resolution is around 0.25 ms. The particle size is limited by the resolution on image anlayzer and the Spin Physics camera recording system. In terms of radiance level measurement, the maximum error is about $\pm5\%$.

Discussion of Results

A series of high-speed motion pictures showing the breakup process of a plane wall jet is given in Fig. 7. Several interesting phenomena of wall-jet evolution and breakup can be noted from these photographs. In Fig. 7a, as the liquid jet traveled along the wall surface in the early stage, the head region diverged in the upward direction. A thin sheet of liquid was formed ahead of the main jet as shown in Fig. 7b. This thin sheet of liquid surface is believed to be caused by shedding phenomena introduced by the inertia of the fast-moving liquid near the free surface of the engulfing wave front. Near the top surface, the velocity of the liquid is much higher than that near the wall since the viscous force is much smaller at the free surface. As time progressed, this sheet became more eivdent, and the head region expanded further (see Fig. 7c). In Fig. 7d, the main jet accelerated and merged with part of the thin liquid sheet. In the later stage, the so-called Klystron effect[21] was visible. (The Klystron effect has been broadly used in electrical
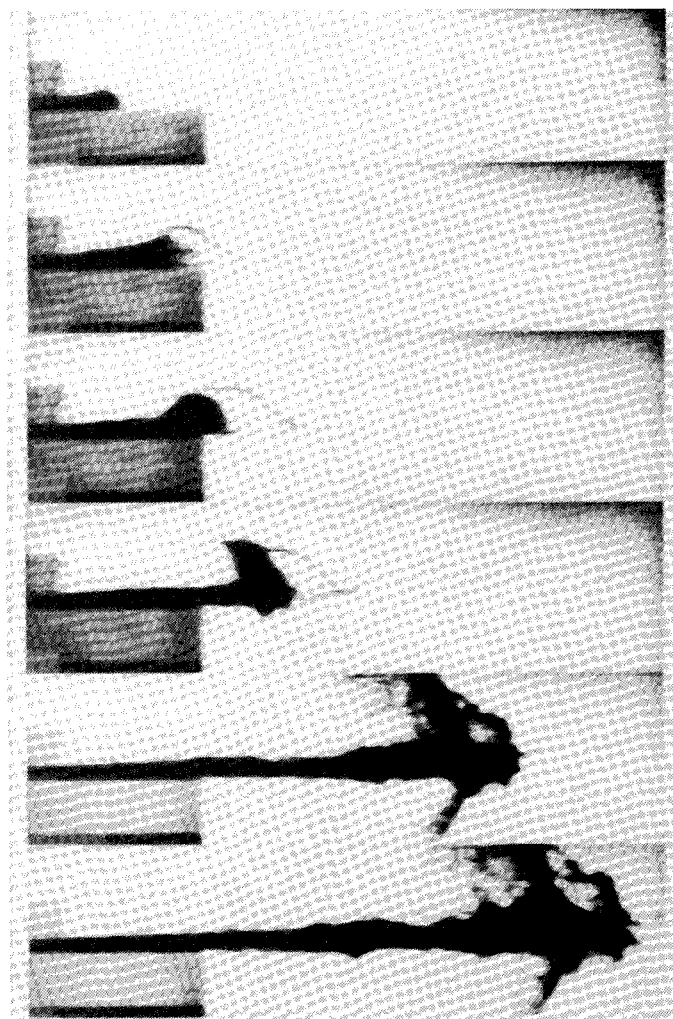

Fig. 7   Interesting phenomena of a plane wall liquid jet breakup process (from high-speed movie film).

systems to explain signal amplifications under high-frequency conditions.) In fluid flow systems, this effect showed the acceleration of the main jet, which provides higher axial momentum fluid at a later time to catch up with the precursor jet mass. Due to the coalescence of the fast and slow moving fluids, the width of the jet spread in transverse directions. This spreading also made the jet-head portion more symmetric. In the meantime, several ligaments and numerous droplets were formed as the head region expanded further. Such a breakup process greatly influenced vaporization, ignition, and combustion of liquid sprays.

A set of high-speed photographs for the free-jet case is shown in Fig. 8. The jet head was quite symmetric as it expanded in the transverse direction. The shape of the jet head changed from a round cross section to a mushroom-shaped contour. The Klystron effect can also be seen in Figs. 8d–8f. The jet head in Fig. 8e became spear shaped with a sharp leading edge. Some ligaments and droplets were formed (see Fig. 8f) near the boundary of the liquid-gas interface.

To demonstrate the differences between conventional high-speed movie film and high-speed x-ray radiography, a set of x-ray movie films showing free-jet breakup processes is given in Fig. 9. It is quite obvious that, unlike the conventional high-speed movie film, the radiance of the jet head region is highly nonuniform. The inner structure of the jet can, therefore, be observed and analyzed from these images.

Figure 10 gives a set of pictures of the same object but with different levels of radiance. The variation in contour of the isophote shows the detailed structure of the nondilute liquid

jet. Although some pulsed x-ray photographs were obtained by Baev et al.,[4] for liquid jet, the detailed inner structure of a nondilute jet during the process of breakup has never been observed before to the best of the authors' knowledge.

Using the Quantex Image Analyzer, the void fraction distribution in the vertical direction (normal to the jet axis) can be deduced for any axial location. Figure 11 shows the void fraction distribution across the widest jet head section (see also Fig. 5 cursor station). Near the centerplane ($y = 0$), the void fraction is much lower than that at the jet boundary [when y is approximately equal to $4H$ (gap width of the jet exit)]. The magnitude of the local void fraction is taken to be proportional to the local pixel value, i.e.,

$$\phi(x,y) = 1 + \frac{1}{mL} \ell_n \frac{I(x,y)}{I_0} \qquad (2)$$

where L is the local interception length. The intensity (pixel value) of pure gas and liquid for Pantopaque in air was 130 and 20 corresponding to the x-ray setting for most tests. It is useful to note that the distance between the x-ray tube head and the image intensifier was held constant during these tests.

A typical void fraction distribution for a wall jet is shown in Fig. 12. It is evident that near the wall ($y/H = 0.5$), the void fraction was almost zero, whereas the value of ϕ was quite close to unity near the outer edge of the wall jet.

A question about the effect of diffraction and scattering from multiple interfaces on the accuracy of Eq. (2) has been addressed. Equation (2) essentially assumes that diffraction and scattering from multiple interfaces have no effect on the reduction of void fraction from intensity measurements. To
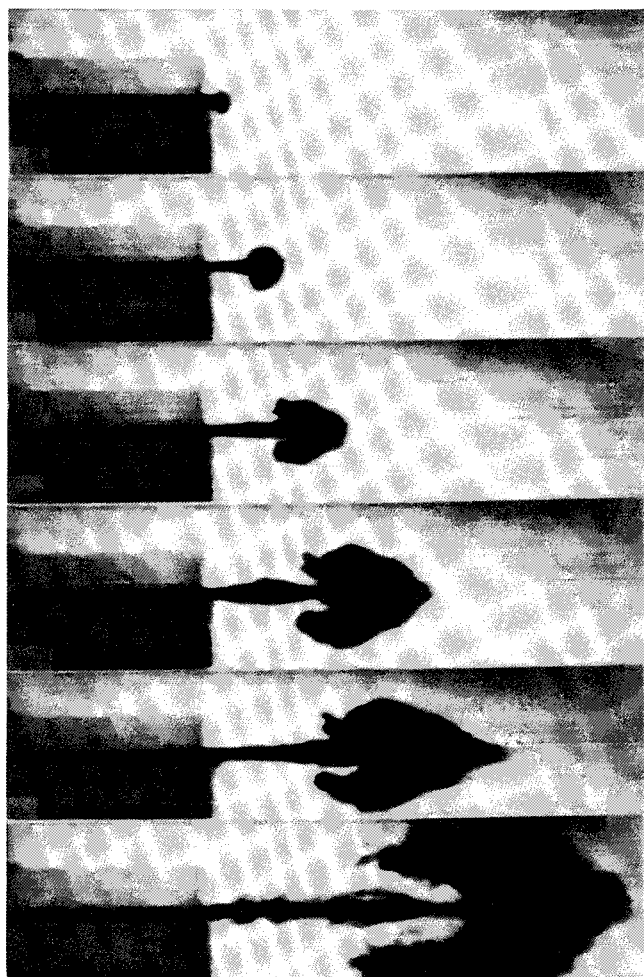

Fig. 8   Evolution of a plane free liquid jet breakup (from high-speed movie film).

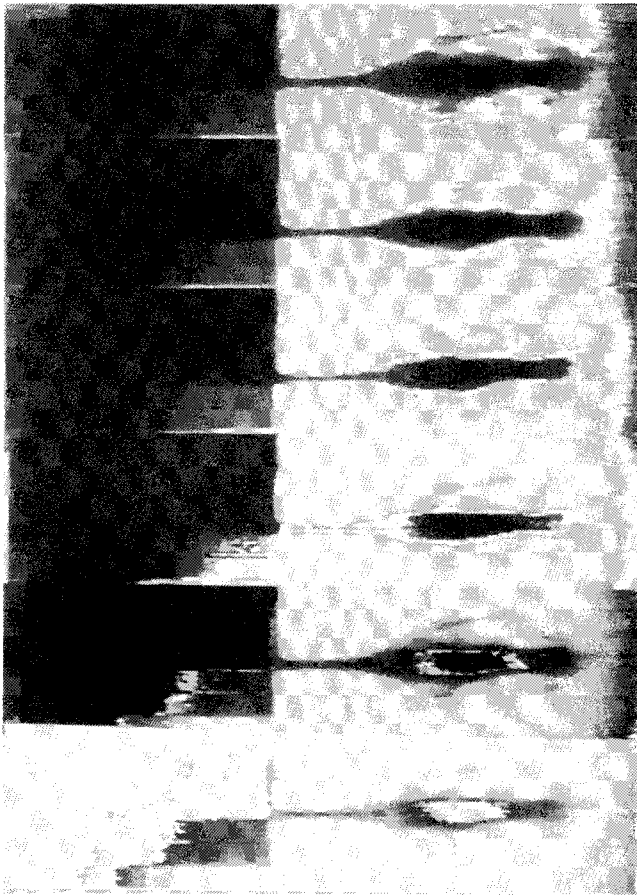Fig. 9   Evolution of a plane free liquid jet using the x-ray radiography system.

Fig. 10 Isophote analysis shows the inner structure of a liquid jet using different x-ray intensity levels.

Fig. 11 Void fraction distribution across the widest jet head region (plane free-jet case).

verify the weak dependence of intensity on the number and orientation of interfaces, two strands of rectangular-shaped solid propellant grains from the same batch with equal length were tested. One strand was cut into 10 sections with different angles to the main axis. The other strand remained as an integral piece. The two strands were placed on a platform adjacent to each other and viewed by x-ray from their end surfaces. The local intensity distribution for each strand was obtained and compared. It was found that the intensity of the uncut piece is only 5.80% higher than that of the chopped strand. This implies that the intensity of the x-ray radiography is minimally affected by the number and orientation of the interfaces. The loaded fraction $(1-\phi)$ deduced from Eq. (2) corresponds to the total width of the liquid intercepted by the x ray.

The jet spreading angle in the y direction is of interest in spray combustion. The angle θ can be determined from the instantaneous jet velocities in both x and y directions. The jet head velocities (u and v) in the x and y directions are deduced from the displacements of the vertical and horizontal lines on the Spin Physics monitor. The spread angle is defined as

$$\theta = 2\tan^{-1}(v/u) \qquad (3)$$

A plot of half spread angle $(\theta/2)$ vs jet head axial velocity (u) is shown in Fig. 13. For both wall- and free-jet experiments, spread angles decrease as jet head velocity increases. This is due to the fact that when a jet has higher axial momentum, the rate of spreading is lower. Based upon the data shown in Fig. 13, the wall-jet spread out more than the free jet due to the momentum distribution effect in the wall jet. Near the wall surface, the nonslip condition must be satisfied, and hence the liquid near the free surface has a higher velocity than the free-jet case for the same jet head velocity.
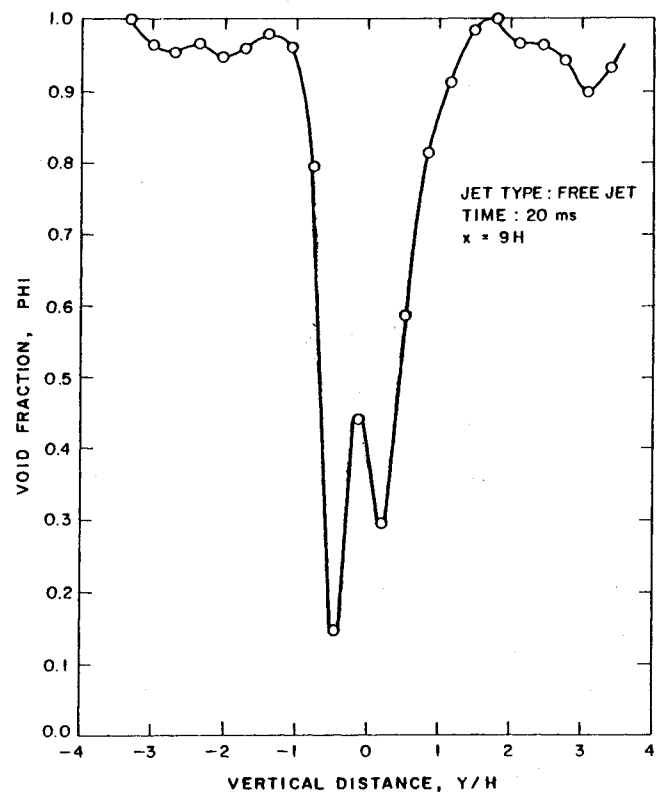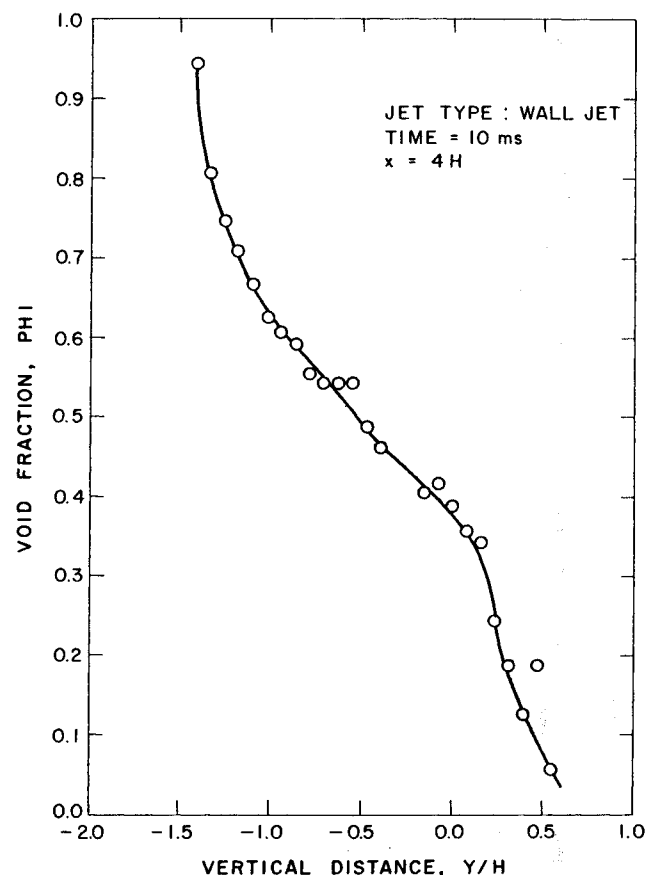

Fig. 12 Void fraction distribution across the widest jet head region (plane wall-jet case).

The jet surface breakup distance (L_{SB}) and the jet core breakup distance (L_{CB}) from the exit station are also important in spray combustion. Figure 14 plots these two distances vs jet head velocity. Determination of L_{SB} was based upon the location of the first discernible divergence of liquid from the jet surface. The value of L_{CB} was determined from the abrupt
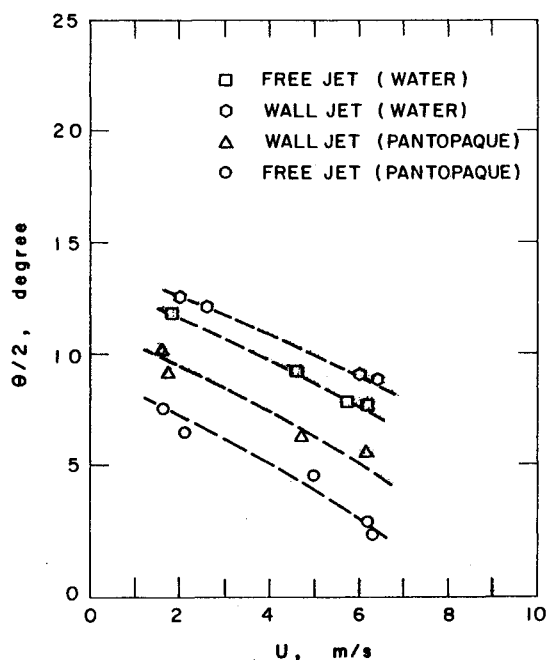

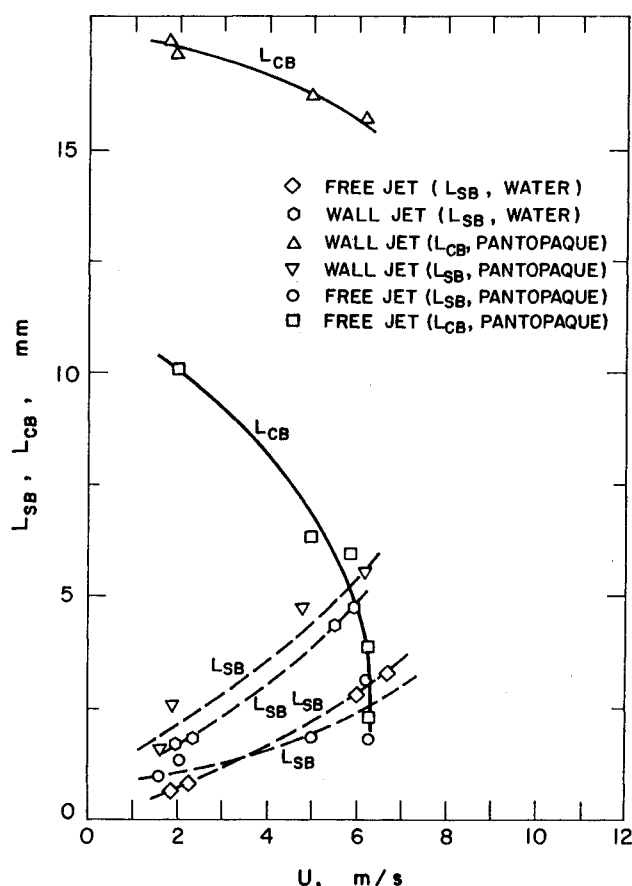Fig. 13   Liquid jet divergent angle under different jet-head velocities.

Fig. 14   Liquid jet breakup length under different jet-head velocities.

increase of intensity along the axial intensity distribution at the centerplane of the jet. For both wall and free jets, L_{SB} increased with jet head velocity due to the higher inertia of the liquid jet which delays the jet surface breakup. However, L_{CB} decreased while jet head velocity increased for both wall and free jets because higher velocity jets may cause droplet collision and coalescence to occur earlier generating an inhomogeneous axial intensity profile. It should be noticed that the jet core breakup distance used here is different from that used in previous studies. (In earlier studies, L_{CB} is the length beyond which the jet is no longer continuous.) At the same jet head velocity, wall jets have longer L_{SB} and L_{CB} than free jets due to the fact that wall jets, which are affected significantly by the stronger viscous force, retard the core breakup. In comparing surface breakup length, at the same value of jet head velocity, the wall jet has lower momentum than the free jet; hence, breakup length is longer.

Summary and Conclusions

The advantages of using real-time x-ray radiography for liquid-jet breakup measurements are summarized as follows:

1) X ray can partially penetrate through the liquid jets, even in the dense regions. Therefore, it is feasible to determine the instantaneous inner structure of the jet in the near-injector region during the jet breakup processes.

2) X-ray radiography is a nonintrusive technique, which does not affect the liquid jet breakup processes and is superior to other methods.

3) The real-time feature of x-ray radiography gives the entire history of the jet breakup event instead of a few snapshots. The x-ray motion pictures taken during the test event can be played back immediately at a lower speed for detailed flow visualization and analysis.

4) All data are in digital form and are convenient for recording, analysis, transfer, and storage in computers.

Based upon the recorded x-ray images analyzed on a digital image processor, jet divergent angle, jet breakup length, and jet void fraction distributions can even be measured in the near-injector region.

The effect of wall friction on the jet breakup process was observed by conducting wall- and free-jet tests. Although the spread angle is larger for the same jet head velocity, longer distances are required for the surface and core to break up in the case of wall jet.

To understand the jet breakup mechanism, more detailed studies are required. Future tests should be conducted under varied conditions, such as different pressure and density levels in the gas phase, higher liquid-jet velocity ranges, various test liquids, different jet nozzle geometries, etc. The development of a comprehensive theoretical model for the near-injector region is also necessary. The predicted results should be compared with experimental data for model validation.

Acknowledgments

References

[1]Arcoumanis, C., and Whitelaw, J. H., "Fluid Mechanics of Internal Combustion Engines: A Review," *International Symposium on Flows in Internal Combustion Engines—III,* Vol. 28, edited by T. Uzkan, W. G. Tiederman, J. M. Novak, American Society of Mechanical Engineers, New York, 1985, pp. 1–17.

[2]Wu, K.-J., Reitz, R. D., and Bracco, F. V., "Measurements of Drop Size at the Spray Edge Near the Nozzle in Atomizing Liquid Jets," *Physics of Fluids,* Vol. 29, 1986, pp. 914–951.

[3]Birk, A., and Reeves, P., "Annular Liquid Propellant Jets—Injection, Atomization and Ignition," U.S. Army Ballistic Research Lab., Aberdeen Proving Ground, MD, BRL Rept., Feb. 1986.

[4]Baev, V. K., Bazhaikin, A. N., Buzukov, A. A., and Timoshenko,

B. P., "Experimental Study of the Development and Structure of High-Velocity Liquid Jets in Air," Vol. 105, edited by J. R. Bowen, J.-C. Leyer, and R. I. Soloukhin, *Progress in Astronautics and Aeronautics,* AIAA, New York, 1986, p. 104.

[5]Shimizu, M., Arai, M., and Hiroyasu, H., "Measurements of Breakup Length in High-Speed Jets," *Bulletin of JSME,* Vol. 27, No. 230, 1984, p. 1709.

[6]Rayleigh, W. S., "On the Instability of Jets," *Proceedings of the London Mathematical Society,* Vol. X, 1879, p. 4.

[7]Rayleigh, W. S., "On the Capillary Phenomena of Jets," *Proceedings of the Royal Society,* Vol. XXIX, 1879, p. 71.

[8]Tyler, E., and Richardson, E. G., "The Characteristic Curves of Liquid Jets," *Proceedings of the Physics Society,* Vol. 37, 1925, p. 297.

[9]Schweitzer, P. H., "Mechanism of Disintegration of Liquid Jets," *Journal of Applied Physics,* Vol. 8, 1937, p. 513.

[10]Merrington, A. C., and Richardson, E. G., "The Breakup of Liquid Jets," *Proceedings of the Physics Society,* Vol. 59, No. 331, 1947, p. 1.

[11]Levich, V. G., *Physiochemical Hydrodynamics,* Prentice-Hall, New Jersey, 1962.

[12]Dombrowski, N., and Hooper, P. C., "The Effect of Ambient Density on Drop Formation in Sprays," *Chemical Engineering Science,* Vol. 17, 1962, pp. 291-305.

[13]Weber, C., "Zum Zerfall eines Flussigkeitsstrables," *Zeitschrift für M. M.,* Vol. 2, 1931, p. 136.

[14]Chaudhary, K. C., and Redekopp, L. G., "The Nonlinear Capillary Instability of a Liquid Jet—Part 1—Theory," *Journal of Fluid Mechanics,* Vol. 96, 1980, p. 2.

[15]Chaudhary, K. C., and Maxworthy, T., "The Nonlinear Capillary Instability of a Liquid Jet—Part 2—Experiments on Jet Behavior Before Droplet Formation," *Journal of Fluid Mechanics,* Vol. 96, 1980, p. 275.

[16]Lafrance, P., "Nonlinear Breakup of a Liquid Jet," *The Physics of Fluids,* Vol. 17, No. 10, 1974, p. 1913.

[17]Lee, H. C., "Drop Formation in a Liquid Jet," *IBM Journal of Research and Development,* Vol. 18, 1974, p. 364.

[18]Nayfeh, A. H., "Nonlinear Stability of a Liquid Jet," *The Physics of Fluids,* Vol. 13, No. 4, 1970, p. 841.

[19]Dukowicz, J. K., "A Particle-Fluid Numerical Method for Liquid Sprays," *Journal of Computational Physics,* Vol. 35, 1980, pp. 229-253.

[20]Ruff, G. A., Sagar, A. D., and Faeth, G. M., "Structure and Mixing Properties of Pressure-Atomized Sprays," AIAA Paper 88-0237, Jan. 1988.

[21]Fenwick, J. R., and Bugler, G. J., "Oscillatory Flame Front Flow Rate Amplifications Through Propellant Injection Ballistics (The Klystron Effect)," Third ICRPG Combustion Conference, Chemical Propulsion Information Agency, Applied Physics Lab., Laurel, MD, No. 138, Vol. 1, Feb. 1967, p. 417.